



## OPEN ACCESS

## EDITED BY

Hailong Li,  
Central South University, China

## REVIEWED BY

Shuanshi Fan,  
South China University of Technology,  
China  
Yongwon Seo,  
Ulsan National Institute of Science and  
Technology, South Korea  
Liu Jianwu,  
Guangzhou Institute of Energy  
Conversion (CAS), China

## \*CORRESPONDENCE

Li Li,  
heu@hrbeu.edu.cn

## SPECIALTY SECTION

This article was submitted to Carbon  
Capture, Utilization and Storage,  
a section of the journal  
Frontiers in Energy Research

RECEIVED 21 June 2022

ACCEPTED 01 August 2022

PUBLISHED 29 August 2022

## CITATION

Wu Q, Lin N, Li L, Chen F, Xv X, Zhang B,  
Wu Q and Liu C (2022), Synergistic  
enhancement of coalbed methane  
hydration process by magnetic field and  
NiMnGa micro-nano fluid.  
*Front. Energy Res.* 10:974647.  
doi: 10.3389/fenrg.2022.974647

## COPYRIGHT

© 2022 Wu, Lin, Li, Chen, Xv, Zhang, Wu  
and Liu. This is an open-access article  
distributed under the terms of the  
[Creative Commons Attribution License  
\(CC BY\)](https://creativecommons.org/licenses/by/4.0/). The use, distribution or  
reproduction in other forums is  
permitted, provided the original  
author(s) and the copyright owner(s) are  
credited and that the original  
publication in this journal is cited, in  
accordance with accepted academic  
practice. No use, distribution or  
reproduction is permitted which does  
not comply with these terms.

# Synergistic enhancement of coalbed methane hydration process by magnetic field and NiMnGa micro-nano fluid

Qiong Wu<sup>1,2,3,4</sup>, Nengyu Lin<sup>2,4</sup>, Li Li<sup>1,3\*</sup>, Feng Chen<sup>1,3</sup>,  
Xianfu Xv<sup>1,3</sup>, Baoyong Zhang<sup>2,4</sup>, Qiang Wu<sup>2,4</sup> and Chuanhai Liu<sup>2,4</sup>

<sup>1</sup>International Joint Laboratory of Advanced Bulk Nanomaterials for Innovative Applications, Harbin Engineering University, Harbin, China, <sup>2</sup>Department of Safety Engineering, Heilongjiang University of Science and Technology, Harbin, China, <sup>3</sup>Institute of Materials Processing and Intelligent Manufacturing, College of Materials Science and Chemical Engineering, Harbin Engineering University, Harbin, China, <sup>4</sup>National Central Laboratory of Hydrocarbon Gas Transportation Pipeline Safety, Heilongjiang University of Science and Technology, Harbin, China

Coalbed methane is an important renewable energy source. Gas hydration technology is a new method for enhancing the utilization of coalbed methane and reducing environmental pollution. Long induction periods, sluggish formation rates, low hydrate yields, and difficulty removing heat during hydrate formation are all issues with gas hydration technology. In this paper, 3 wt% NiMnGa (NMG) phase-change micro/nanoparticles and 0.05% sodium dodecyl sulphate (SDS) were compounded, and gas hydration experiments were conducted under various initial pressures and gas sample conditions to investigate. The findings revealed that NMG has efficient mass transfer properties as well as phase-change heat absorption properties, which significantly improved the kinetic process of the gas hydrate by mass and heat transfer, shortened the induction time, increased gas consumption, and increased the gas consumption rate during the rapid hydrate growth period. When the initial pressure was 6.2 MPa, the induction time was reduced by 89.26%, 92.48%, and 95.64%, and the maximum gas consumption rate was increased by 238.18%, 175.55%, and 113.60%, respectively, when using different concentrations of methane in the NMG-SDS system compared to the pure SDS system. The NMG used in this paper showed potential for future use in mixed gas hydration technology.

## KEYWORDS

coalbed methane, gas hydration, phase-change micro/nanoparticles, NiMnGa, kinetic characteristics

## 1 Introduction

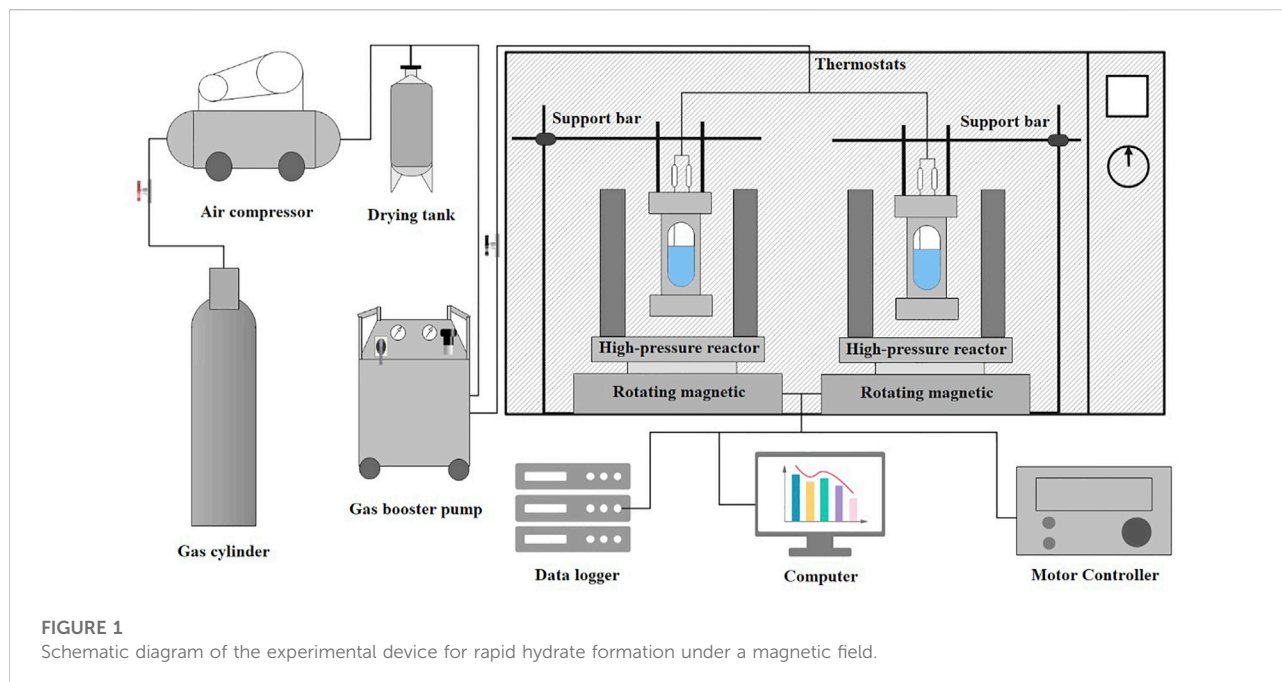
Coal mine methane (CMM), also known as coalbed methane (CBM), is an important source of unconventional natural gas resources and clean energy, consisting primarily of methane and air (Gaikwad et al., 2021). The Intergovernmental Panel on Climate Change (IPCC) has clearly stated that methane, a coal-related gas, has a 20-years global warming potential (or warming effect) 86 times greater than that of carbon dioxide in the 20 years following emissions. Releasing coal mine methane directly into the atmosphere is not only a waste of resources but also a greenhouse effect (George et al., 2020). Therefore, it is important to accelerate the development and utilization of coal mine methane to increase the supply of clean energy and reduce the emission of greenhouse gases (Yuan, 2021). The low concentration of methane in CBM can be separated from CBM by different conventional gas separation processes (Gaikwad et al., 2021), and the main gas mixture separation methods include pressure swing adsorption (Gao et al., 2021; Tian et al., 2021), low-temperature separation (Yang et al., 2020), and membrane separation (Jiang et al., 2021). A gas hydrate is an ice-like hydrate that forms when water reacts with gas components at a specific temperature and pressure. Based on the mild formation conditions (pressurized synthesis above 0°C), high gas content (164 times the volume of methane gas can be stored in 1 g of hydrate), and safe storage (stable storage at normal pressure, from -15 to -10°C) of gas hydrates, scholars have proposed the gas hydrate solidification method (Veluswamy et al., 2018). Conducting gas hydration research can facilitate the development of hydration separation processes and expand the use of low-concentration gas, thus reducing the environmental losses caused by the direct discharge of low-concentration gas, making effective use of coal mine gas, and alleviating energy shortages. However, due to issues such as a long induction time, slow formation rate, low hydrate yield, and difficulty removing the heat of hydrate formation, it is difficult to form gas hydrates quickly using industrial methods.

Heat and mass transport parameters are the primary limiting factors in the gas hydration process. The gas hydration process can be significantly enhanced by enhancing the heat and mass transport conditions of the process. Currently, dynamic strengthening techniques or static strengthening techniques are generally used to promote hydrate formation. Dynamic strengthening techniques mainly include agitation (Ren et al., 2020), bubbling (Cheng et al., 2021), spraying (Zhong et al., 2010), and ultrasonication (Sun and Fan, 2005). Static strengthening techniques include the addition of surfactants such as sodium dodecyl sulphate (SDS) (Chaturvedi et al., 2021), alkyl polyglycolide (APG) (Chen, 2020), sulfonated lignin (SL) (Yi et al., 2019), and porous media (Zhang et al., 2021a) such as silica (Zhang et al., 2020; Huang et al., 2021) and montmorillonite (Zhang et al., 2018). To some extent, these techniques can aid in the formation of hydrates. However, the

formation of gas hydrates is an exothermic reaction, and the hydration reaction releases a significant amount of heat when hydrates form rapidly. The heat retained in the reaction system that is not rapidly diffused and transferred perturbs the temperature stability of the hydration system, thus affecting the overall reaction and preventing further hydrate formation (Yoslim et al., 2010).

In recent years, many scholars have considered the use of nanofluids to promote the heat and mass transfer processes of hydrates. Nanofluids have unique mass and heat transfer properties, such as high specific surface area (Zhou, 2016), active Brownian motion (Cui et al., 2017), small size (Su et al., 2008; Xia et al., 2016), and controlled concentration (Pahlavanzadeh et al., 2016; Liu et al., 2017), that are expected to rapidly enhance the heat and mass transfer processes of gas hydration. Song et al. (Song et al., 2021) used carbon nanotubes (CNTs) as carriers and covalently grafted the functional -SO<sub>3</sub>-group (like the hydrophilic group in SDS) onto the surface of the nanocarriers; the SCNT nanofluid's methane storage reached 142 v/v in methane hydrate formation. Wu et al. (2021) produced Fe<sub>3</sub>O<sub>4</sub> nanoparticles and surface modified them with sodium oleate (SO) and SDS bilayers, the composite-promoted system demonstrated a significant increase in methane storage capacity and hydrate formation rate. In addition, due to the regular arrangement of SDS&SO@Fe<sub>3</sub>O<sub>4</sub>, a magnetic field was successfully introduced into the reaction system, which further enhanced hydrate formation. Zhang et al. (2021b) immobilized silver nanoparticles on activated carbon; the unique heat transfer properties of silver and the presence of Ag nanoparticles significantly aided in overcoming this limitation by enhancing external nucleation, and Ag-NP@AC significantly reduced the hydrate induction time.

An analysis of the above-related studies reveals that the current studies on nanofluids are focused mainly on single or binary gas compositions, such as CH<sub>4</sub>, CO<sub>2</sub>, and C<sub>2</sub>H<sub>6</sub>, and less on the kinetics of hydrate formation from multiple gas compositions in nanofluids. In addition, the positive effects of nanofluids on gas hydrates occur mainly in the area of mass transfer. Although heat transfer is improved, it is difficult to rely only on heat conduction by nanoparticles for further improvements. Ni-Mn-based phase-change alloys are magnetic shape-memory materials that undergo thermoelastic martensitic transformation with a large latent heat of phase change (Manfred et al., 2000; Lyubina, 2017); an increase in temperature can induce a structural transformation from martensite to austenite, i.e., reversible martensitic transformation (Chen et al., 2006; Ma et al., 2009). The transformation of the crystal structure requires the absorption of external heat, which results in a lower ambient temperature. The temperature and latent heat of the reverse martensitic transformation can be controlled by appropriate adjustment of the stoichiometric ratio of each element in Ni-Mn-based alloys and the addition of other alloying elements (Chen et al., 2006; Yu et al., 2007). In



recent years, some scholars have found that the preparation of polycrystalline materials is simpler and more practical than that of monocrystalline materials. Among them, the NMG ferromagnetic shape-memory alloy is not only a thermoplastic shape memory alloy controlled by a temperature field but also has the advantages of a fast response and large recoverable strain (Tian et al., 2009; Fan et al., 2021). They show promise as a way to reduce the time it takes for hydrates to form, increase the gas storage capacity and rate of hydrate formation, and accomplish fast formation in industrial applications. In this paper, NMG phase-change alloys and micro/nanoparticles were prepared. A uniformly dispersed stable fluid of NMG was made in reactor by using SDS and an external rotating magnetic field. Since the inverse phase transition temperature of NMG is around 2°C, the phase equilibrium pressures of the three gas samples at the initial temperature of 2°C were calculated (Supplementary Table S1). Based on phase equilibrium conditions, kinetic experiments on gas hydrate formation in NMG micro/nanofluids were carried out at initial pressure of 6.2, 7.2, and 8.2 MPa, and different gas samples were analysed to construct an exotherm during the rapid formation of hydrate and induce the reverse martensitic transformation of NMG to remove heat and promote the formation of gas hydrate. The experimental data and results of this study are useful for understanding the kinetics of NMG-enhanced gas hydrate formation, and the method is expected to open up new possibilities for using phase-change micro/nanoparticles in gas hydration solidification technology.

## 2 Experiment

### 2.1 Experimental materials and apparatus

Sodium dodecyl sulphate was supplied by Tianjin Guangfu Fine Chemical Research Institute. NMG powder with a median particle diameter of 18.7 μm was ball-milled in a high-speed vibratory ball mill (model GB-80, Nanjing Boyuntong Instrument Technology Co., Ltd.). Beijing Beiyang Special Gas Research Institute Co. Ltd. provided the gas and high-purity nitrogen. The test water is pure Class II water that has been purified by Thermo Fisher Scientific.

The experimental apparatus for the rapid formation of hydrates under the action of a rotating magnetic field was composed of five parts: a high-pressure reactor, a magnetic steel rotating platform, a high- and low-temperature thermostat, a temperature sensor (PT100, Class B), a pressure sensor (DPI 701-E51GAP-F, Elbaissde) and a data collection system. The experimental apparatus is shown in Figure 1. The effective volume of the reactor was 100 ml, and the reactor body was made of titanium alloy to ensure stable magnetic field strength. The rotating speed range of the platform is 0–200 r/m, and the two ends of the platform are equipped with two magnetic steels, which can provide 0–0.5 T magnetic field. Based on their magnetic characteristics, the magnetic particles were suspended in solution in the autoclave by a rotating magnetic field that stirred as well as dispersed the particles.

## 2.2 Experimental procedure

NMG-SDS suspensions and SDS suspensions were prepared. Then, the zero points of the temperature and pressure sensors were calibrated before the start of the experiment, and the gas tightness of the device was checked using nitrogen gas. The gas tightness of the reactor was judged good if the change in pressure within 2 h was less than 0.01 MPa. The following were the steps in the experiment: 1) The reactor was cleaned three times before the experiment with purified water prepared in this facility. The prepared reaction solution (40 ml) was added to the reactor after drying. The temperature sensor, inlet line, and pressure sensor were all connected. 2) The thermostat was set to the desired temperature, and the data gathering system was activated to track temperature and pressure changes. The reactor was purged three times with CH<sub>4</sub> of roughly 2 MPa, and methane was injected into the reactor to achieve the initial pressure value, once the temperature shown by the data collector reached the predetermined temperature. 3) Regulate the magnetic field strength to 100 mt and the rotation speed to 100 r/m respectively, and the magnetic steel rotating platform starts to rotate. 4) When the temperature began to rise and the pressure began to fall, methane hydrate started to form. After the reaction was conducted for a period of time, the temperature and pressure curves started to level off and stabilized without meaningful changes for 30 min. The hydration reaction process was regarded complete when the gas hydrate was totally produced. In this paper, we investigated the effect of different initial pressures and gas samples on the formation of gas hydrates by NMG. Each experiment was repeated three times to lessen the unpredictability of the results.

## 2.3 Characterization

The microscopic morphology of NMG and the dispersion of NMG in pure water and SDS solutions were observed using scanning electron microscopy (SEM) at an accelerating voltage of 20 kV with an FEI Quanta 250, United States. To test the suspension and dispersion effect of SDS, the suspension time of NMG in different systems was measured. The average diameter of NMG particles was obtained by a Malvern Mastersizer 3,000 E laser particle size analyser manufactured by Malvern, United Kingdom.

## 2.4 Data processing methods

The hydrate formation induction time is an important metric for determining the rate of hydrate formation. The induction time was measured from the initial equilibrium state to the first significant increase in temperature and reduction in pressure during the hydration reaction in this investigation. Methods of calculating gas consumption and consumption rate can be found in the supporting information.

## 3 Results and discussion

### 3.1 Characterization of NMGs

Micro/nanoparticles easily undergo absorption and agglomeration. In order to analyze the improved mass transfer behavior of micro/nanofluids, it is critical to produce uniform and stable dispersion of micro/nanoparticles. The surface structure of NMG micro/nanoparticles and their state of dispersion and agglomeration in different solutions were characterized by SEM at an accelerating voltage of 20 kV. Scanning electron micrographs of NMG particles in [Figures 2A2,A3](#) show an irregular polygonal structure. Part of the surface has a smooth serrated appearance that can provide a large nucleation site for the formation of hydrate crystals. [Figures 2B2,B3](#) show SEM micrographs of the degree of dispersion of NMG particles in the pure water system, which can be seen to appear in a bonded state from particle to particle. And in [Figures 2C2,C3](#), the SEM micrographs show the dispersion state of NMG in the SDS solution system, and the addition of SDS can effectively solve the bonding state between NMG particles and put them in a uniformly dispersed state.

The state of NMG in pure water is shown in [Figure 2A1](#). When NMG is added to pure water, they agglomerate and form a deposit at the bottom of the beaker. [Figures 2B1,C1](#) are photographs of the dispersed state of the NMG-pure water system and NMG-SDS system after stirring by the disperser and standing for 500 min. Because the density of NMG was greater than that of the base solution, some of the particles agglomerated and deposited at the bottom of the beaker despite the disperser stirring and dispersing the NMG-pure water system. When NMG particles were added to the SDS solution, SDS molecules adsorbed on the surface of the micro/nanoparticles, and the particles, even if aggregated, formed a stable dispersion. [Figure 2D](#) shows histograms of the final suspensions and dispersion time for the NMG-pure water system and the NMG-SDS system. The addition of SDS greatly enhanced the suspension and dispersion of NMG; the final suspension and dispersion time of the NMG-SDS system increased by 53.33% compared with that of the NMG-pure water system.

The particle size distribution curves of NMG particles obtained by a laser particle size analyser, shown in [Figure 2E](#), have a median diameter D<sub>50</sub> of 18.7 μm and a dispersion D<sub>60</sub>/D<sub>10</sub> of 3.15.

### 3.2 Characterization of the gas hydrate formation process in NMGs

Experiments on the kinetics of gas hydration processes were carried out in the experimental equipment for rapid hydrate formation under the action of a rotating magnetic field by NMG for various gas mixtures at varied beginning pressures.

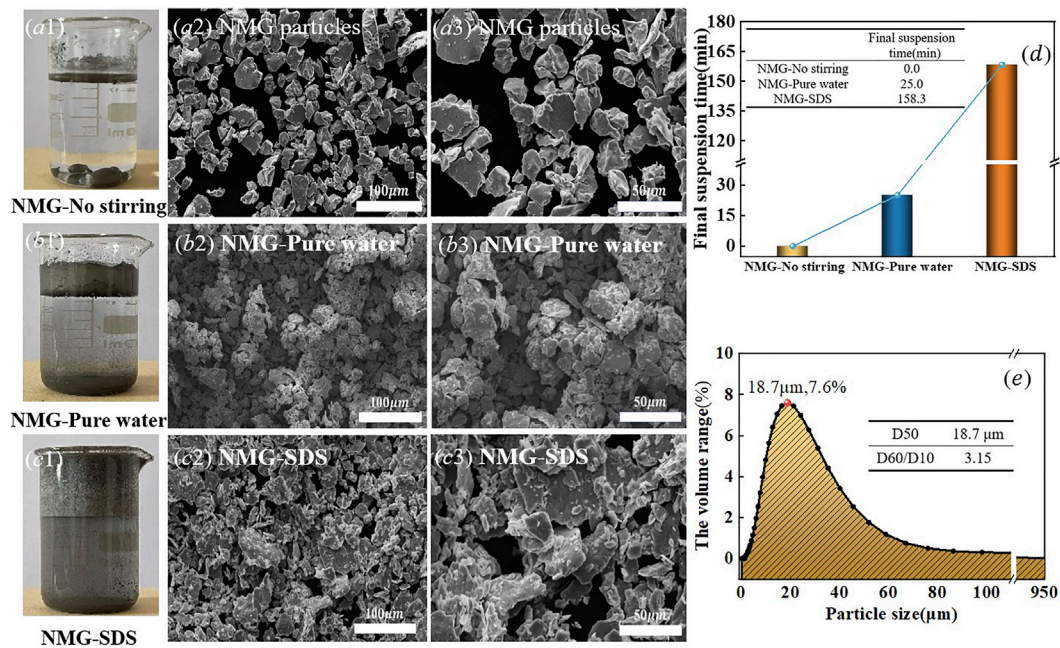
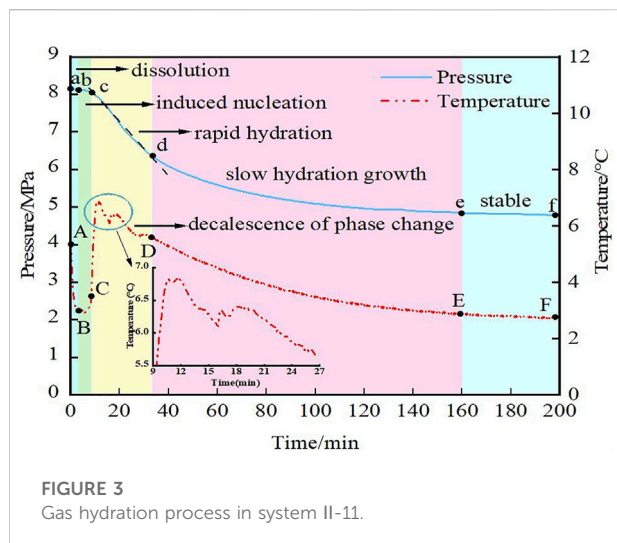


FIGURE 2 Characteristic test results of NMG micro/nanofluids.

TABLE 1 Experimental conditions and formation results of gas hydrates under different conditions.

System	Gas	Material	T/ °C	P/ MPa	No.	Induction time/min	Gas consumption/ mmol of gas/mol of water	Average gas consumption rate/ mmol of gas/mol of water·min <sup>-1</sup>	Hydrate phase concentration	Residual gas concentration/%
I	G1	SDS + NMG	2	6.2	I-1	121.1	10.098	0.060	34.056	24.653
					I-2	9.7	10.604	0.063	32.463	26.094
					I-3	9.1	19.471	0.079	37.233	26.021
					I-4	5.3	29.411	0.091	37.091	25.711
II	G2	SDS + NMG		6.2	II-1	43.5	17.022	0.071	39.022	29.558
					II-2	9.1	18.379	0.076	36.975	31.066
					II-3	8.1	32.670	0.144	39.106	30.490
					II-4	3.4	41.453	0.155	38.670	31.190
III	G3	SDS + NMG		6.2	III-1	17.0	24.975	0.148	40.873	31.636
					III-2	4.9	29.129	0.180	41.081	31.636
					III-3	4.2	42.199	0.203	39.287	36.776
					III-4	2.6	52.018	0.221	39.827	33.551



Experiments with 3 wt% NMG were conducted out at beginning pressures of 6.2, 7.2, and 8.2 MPa, respectively, at a temperature of 2°C. Experiments on gas hydration formation were done out on three different gas samples (G1: 60% CH<sub>4</sub>, 32% N<sub>2</sub>, 8% O<sub>2</sub>; G2: 70% CH<sub>4</sub>, 24% N<sub>2</sub>, 6% O<sub>2</sub>; G3: 80% CH<sub>4</sub>, 16% N<sub>2</sub>, 4% O<sub>2</sub>). Each experiment was performed three times to reduce experimental error, and the experimental circumstances and average experimental findings of gas hydrate formation experiments under various settings are presented in Table 1. Supplementary Table S2 compares the kinetic characteristics of gas hydrate formation for different systems and shows the experimental data for all experimental systems. For system II-11, the temperature-pressure profile changes during gas hydrate production, and the stage analysis diagram is shown in Figure 3.

The gas hydration process has 5 main phases: gas dissolution, induced nucleation, rapid hydration growth, slow hydration growth, and stabilization (Kang et al., 2018), as shown in Figure 3. After filling the reactor at the pressure set in the II-11 experiment, the gas inlet was closed, and the initial pressure was reached at point a. The external work of the compressed gas caused an increase in the internal energy of the reactor, which led to an increase in temperature at point A. Due to the cooling effect of the external thermostat system, the temperature dropped rapidly to point B after the inlet was completed until the internal and external temperatures of the reactor reached equilibrium and remained stable. Within 5 min, the reaction indicated a significant pressure reduction at point b, which was caused by methane gas solubility in the liquid phase. After the end of the gas dissolution period (ab phase), the pressure and temperature were constant for a period of time, which was defined as the induction time, i.e., the induced nucleation phase (bc phase). The induction time for this group of experiments was only 3.33 min, indicating that the hydrate started to form in a very short period of time. The guest

molecule CH<sub>4</sub> dissolved in the liquid phase entered the gas-liquid interface for the hydration reaction during the cd phase, which was a period of fast hydrate development. Because NMG particles have a large specific surface area, they provide a broad contact area for the gas-liquid reaction, which considerably improves mass transfer efficiency. The hydrate crystals nucleated rapidly to form a hydrate, releasing a large amount of heat, which showed that the pressure curve obviously decreased to point c in Figure 3, and the temperature curve increased to point C in Figure 3. The reverse martensitic transformation of the NMG particles was induced by the temperature rise, the phase transformation process absorbed the heat generated by hydrate formation and lowered the system temperature, the temperature curve showed a downwards concave trend (i.e., the enlarged part circled in the figure), and the ambient temperature enhanced hydrate formation even more. The de phase was the slow growth period of hydrate. The pace of hydrate formation slowed during this time, the temperature began to fall slowly from point D, and the pressure began to fall slowly from point d. When the hydrate was fully formed, the temperature-pressure curve tended to be constant with the ambient temperature during the ef phase.

### 3.3 Effect of methane concentration and initial pressure on hydrate growth

Typical curves of temperature and pressure versus time for different gas hydration processes for different systems at 6.2, 7.2, and 8.2 MPa are shown as Supplementary Figure S1 in the supplementary material. The temperature-pressure curves show the differences in induction time for various systems. In the SDS system, the induction time was clearly observed, while the presence of NMG drastically shortened the induction time, and the induction time was not visible. By using the pressure drop, the temperature-pressure curve can be used to determine the amount of gas hydrate generation in various systems, and the slope of the temperature-pressure curve can be used to determine the rate of gas hydrate generation. The initial temperature of the whole experiment was 2°C, and the ambient temperature in the reactor was kept constant to prevent the solution from forming a mixture of ice and water. The whole experiment lasted for 5 h. Kinetic parameters such as induction time, gas consumption, gas consumption rate, and methane recovery rate were evaluated to compare the differences in hydrate formation effects in different systems.

#### 3.3.1 Induction time

One of the most useful parameters for determining whether gas hydrates may be created quickly is the induction time. The time necessary for hydrate nucleation can be effectively reduced by reducing the induction time. (Liu N et al., 2021). After the gas

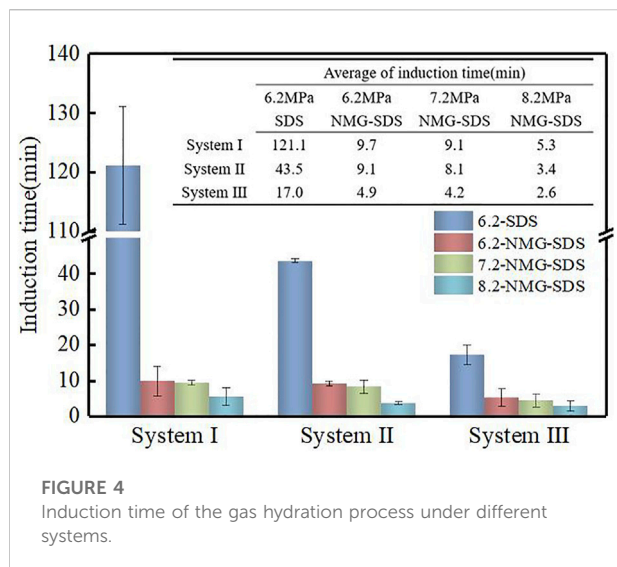


**FIGURE 4**  
Induction time of the gas hydration process under different systems.

dissolves and a slight pressure drop occurs, the temperature and pressure remain constant for a period of time. In this experiment, the induction time is specified as this period. Figure 4 shows the graph of induction time for the gas hydration process in different systems. The findings suggest that adding NMG to the gas hydrate formation process can significantly reduce the induction time and improve the promotion effect. For the different systems, the average induction periods for hydrate formation employing NMG at an initial pressure of 6.2 MPa were 9.7, 9.1, and 5.3 min, respectively. The average induction times (121.1, 43.5, and 17.0 min) were reduced by 91.99%, 79.08%, and 68.82%, respectively, compared to the induction time in the pure SDS system. In addition, the induction time showed a gradual shortening trend with increasing initial pressure and methane concentration. Comparing the three different systems, the shortest induction time of gas sample G3 was 2.6 min when the initial pressure was 8.2 MPa. NMG has a large specific surface area, which can provide nucleation sites to speed up hydrate nucleation, enhance gas-liquid contact area, and improve gas-liquid mass transfer (Sun et al., 2019), so it does not affect the growth of nucleation and does accelerate the formation of hydrate. When many SDS active groups adsorb on NMG to form micro/nanofluids, the gas-phase and aqueous-phase active groups are separate. Without micro/nanofluids, intermolecular interactions are stronger than those between gas and water molecules. Furthermore, the presence of SDS reduces surface tension at the gas-liquid interface, promotes methane gas dissolution, increases the driving force for hydrate formation, improves mass transfer conditions, accelerates hydrate formation, and increases the hydrate nucleation rate (Liu Z et al., 2021; Song et al., 2021).

### 3.3.2 Gas consumption

Gas consumption is an important metric for assessing the storage impact of gas hydrates as well as the gas content (Yin et al., 2020), and it is calculated by Equation (S1). Figure 5 shows the gas consumption during gas hydration in different systems. Where, the dashed part indicates the maximum gas consumption in different systems. The average gas consumption required for NMG hydrate formation at 6.2 MPa is 10.604, 18.379, and 29.130 mmol of gas/mol of water in different systems, compared to the average gas consumption of the pure SDS system (10.248, 17.022, and 24.975 mmol of gas/mol of water), which is an increase of 3.47%, 7.97%, and 16.43%, respectively. In addition, the gas consumption increased with increasing CH<sub>4</sub> concentration and initial pressure. When the initial pressure was 8.2 MPa, the gas consumption reached the highest value of 52.018 mmol of gas/mol of water using G3, which was 165.97% higher than that using the G1 system (29.411 mmol of gas/mol of water) and 114.89% higher than that using the G2 system (41.450 mmol of gas/mol of water). The presence of micro/nanoparticles clinging to bubble surfaces in the liquid phase makes the bubbles more stable and less likely to coalesce, as well as increasing the gas-liquid contact area, which provides more nucleation sites (Liu et al., 2020). The high thermal conductivity and phase-change properties of NMG can rapidly dissipate heat from the hydration reaction, thus accelerating the solution velocity and formation rate. The micro/nanoparticles undergo continuous Brownian motion, which can regenerate the gas-liquid interface and expand the gas-liquid contact area, allowing methane to diffuse more easily (Song et al., 2021). Under the influence of an external magnetic field, these activities can create a good stirring effect. The hydrates generated at the gas-liquid interface are mixed into the solution and nucleated as the gas phase continues to enter the water to form hydrates, and the hydrate fragments enter the liquid phase to speed up nucleation. Figure 6 depicts the gas consumption curves for various systems over time. According to the findings, as the concentration of CH<sub>4</sub> in the solution rises, more CH<sub>4</sub> molecules enter the solution to participate in the process. As a result, the hydrate quickly forms a thick hydrate layer on the solution surface, and the hydrate surface becomes denser due to multiple formation, decomposition, and generation processes. At the same time, the higher initial pressure provides enough driving force for the hydrate formation process, which can reduce the induction time required for hydrate formation, allowing for the formation of multiple hydrates in a short period of time and increasing gas consumption.

### 3.3.3 Gas consumption rate

The gas consumption rate is one of the criteria used to judge the rapid and very large formation of gas hydrate. Figure 7 depicts the gas consumption rates in various systems during the gas hydration process. At 6.2 MPa, the maximum gas consumption rates of NMG-SDS in different systems were

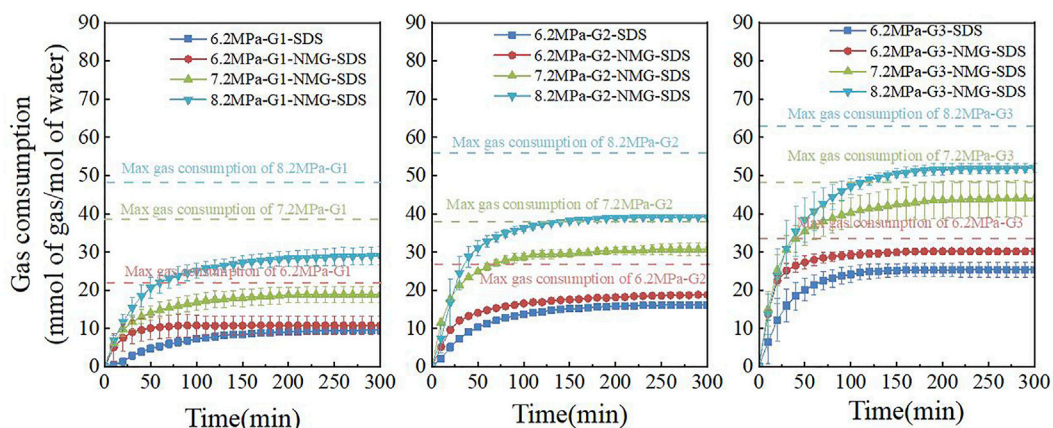


**FIGURE 5**  
Gas consumption during gas hydration of different gas components under different systems.

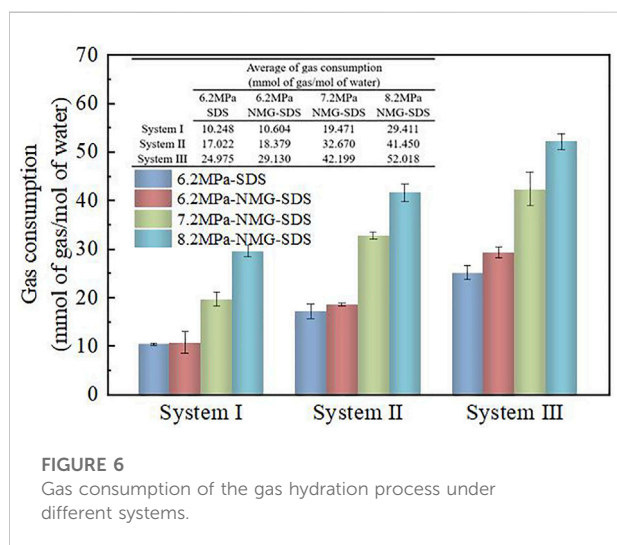


**FIGURE 6**  
Gas consumption of the gas hydration process under different systems.

0.167, 0.284, and 0.558 mmol of gas/mol of water·min<sup>-1</sup>, respectively, which increased by 238.18%, 175.55%, and 113.5% compared with the pure SDS system (0.050, 0.103, and 0.261 mmol of gas/mol of water·min<sup>-1</sup>). Furthermore, as initial pressure and methane concentration increased, the maximum gas consumption rate increased. Figure 8A depicts the average gas consumption rates of the gas hydrate process in various systems, with hydrate formation rates of 0.063, 0.076, and 0.181 mmol of gas/mol of water·min<sup>-1</sup> using NMG at 6.2 MPa for various gas sample systems. The average gas consumption rate of NMG increased by 5.22, 7.64, and 21.88 percent, respectively, when compared to the average gas consumption rate of the pure SDS system (0.060, 0.071, 0.148 mmol of gas/mol of water·min<sup>-1</sup>). The gas consumption rate gradually increased with increasing CH<sub>4</sub> concentration and increasing initial pressure. When the initial pressure was 8.2 MPa, the gas

consumption rate was 0.221 mmol of gas/mol of water·min<sup>-1</sup>, which was 56.87 percent faster than when the initial pressure was 6.2 MPa (0.091 mmol of gas/mol of water·min<sup>-1</sup>) and increased by 143.07 percent over the G1 system (0.063 mmol of gas/mol of water·min<sup>-1</sup>). The gas consumption rate of the gas hydrate process was high at first, then gradually decreased and stabilized, owing to the fact that CH<sub>4</sub> gas is soluble in water, and SDS reduced the surface tension of the solution, allowing the gas to be more soluble in water. T80 was defined in this experiment as the time required to form 80 percent of the hydrate, as shown in Figure 8B. In the G1-NMG-SDS system, 80% of the hydrates was formed 30 min after the induction period, while in the G1-SDS system, 80% of the hydrates formed only 115 min after the induction period. Therefore, the addition of NMG promoted the rapid formation of hydrates during the fast growth period.

Because NMG has a large specific surface area, active Brownian motion, a small volume, and a controllable concentration, it can provide more active sites for the hydrate nucleation process, effectively shorten the induction time of gas hydrate formation, and accelerate the gas consumption rate early in the gas hydration process. The phase-change material can absorb external heat when the phase change occurs, thus lowering the ambient temperature, eliminating the heat generated during hydrate formation in time, and enhancing the heat transfer during the gas hydration separation process. Based on the magnetic property of NMG, the peripheral rotating magnetic field can realize the suspension and stirring of NMG. Due to the high specific surface area of micro/nanofluids (as the heat exchange area between particles and fluid increases, heat transfer is accelerated, providing more reaction interfaces and increasing nucleation rates), active Brownian motion (as Brownian motion causes particles to collide with each other in the gas-liquid boundary layer, it reduces the thickness of the mass

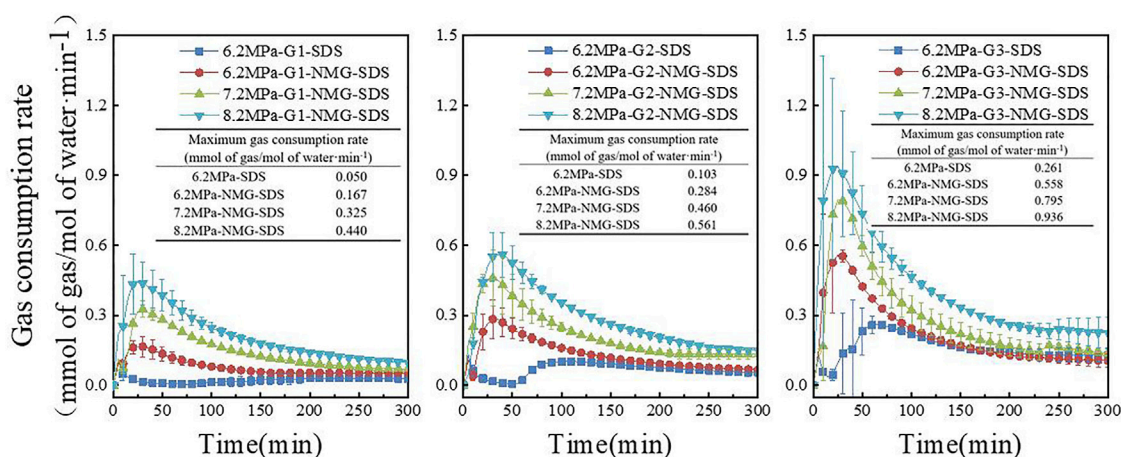


FIGURE 7 Gas consumption rate during gas hydration of different gas components under different systems.

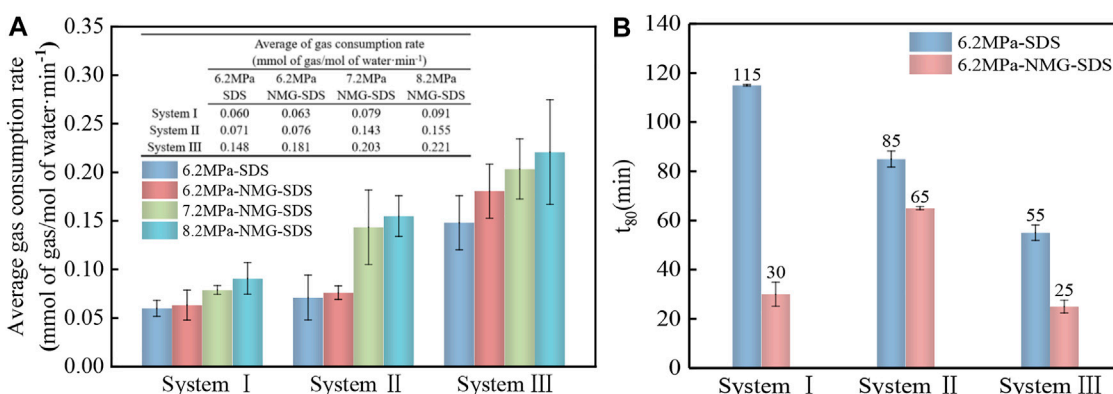


FIGURE 8 Gas consumption rate during gas hydration of different gas components under different systems.

transfer boundary layer and changes the hydrodynamic properties of the surrounding liquid phase). The suspended particles' small size, which is less than the thickness of the gas-liquid mass transfer boundary layer, allows them to cross the gas-liquid boundary layer under the effect of osmosis, reach the gas-liquid interface, adsorb gas molecules, and then return to the liquid phase body to achieve gas transport. As a result, the controlled concentration can speed up the gas hydration separation mass transfer process. Furthermore, adding SDS to the solution can improve the suspension effect, enhancing the heat and mass transfer processes in micro/nanofluids.

### 3.3.4 Methane recovery

Gas chromatography was used to obtain the hydrate separation and purification concentration and the recovery rate of the relevant experimental system. In the process of gas

separation and purification by the hydrate method, the effective release and recovery of methane from hydrates is also a key step in the industrialization of hydrate separation and purification technology. In the industrial application of gas hydrate separation and purification technology, the higher the recovery of hydrated methane, the more valuable the reaction system and reaction circumstances are.

Figure 9 shows the graphs of methane recovery during gas hydration for different gas compositions at an initial pressure of 6.2, 7.2, and 8.2 MPa. The recovery rate of CH<sub>4</sub> gradually increased with increasing methane concentration and increasing initial pressure. In the G3 system, the maximum methane recovery rate was 55.87% at a initial pressure of 8.2 MPa, which was 44.29% higher than that at a initial pressure of 6.2 MPa (38.72%) and 37.51% higher than that in the G1 system (40.63%). The experimental results demonstrated

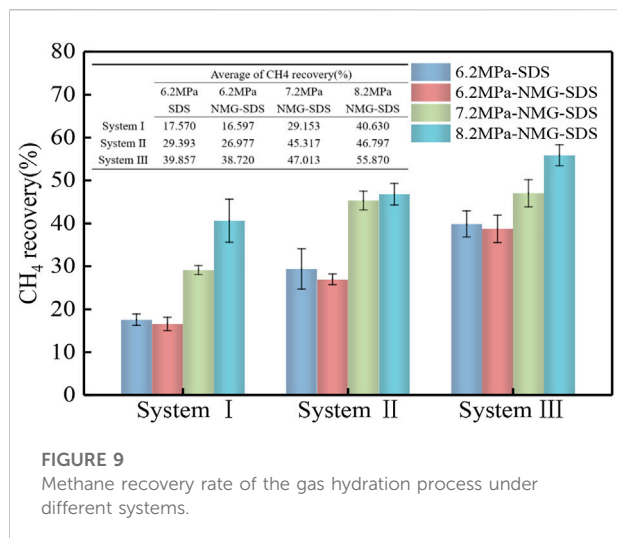


FIGURE 9  
Methane recovery rate of the gas hydration process under different systems.

that, under the same driving power, CH<sub>4</sub> recovery increased as the methane content in the gas rose.; the higher the methane content in the gas was, the better the gas purification capacity after the hydration separation reaction. However, the NMG system seemed to have no significant effect on methane recovery.

### 3.4 Analysis of the enhanced mechanism of gas hydrate formation in NiMnGa micro/nanofluids

NMG has a huge specific surface area and surface activity. The irregular and jagged metal surface can provide more nucleation sites for hydrates, which can promote hydrate nucleation and shorten the induction time. In addition, the larger specific surface area can also increase the gas-liquid contact area, which means more methane molecules can enter the liquid phase and participate in the reaction (Zhou et al.,

2014). NMG as a metal particle has strong thermal conductivity, which can help the thermal conductivity of the liquid (Liu et al., 2020) and accelerate the removal of the heat of hydration generated during hydrate formation. Importantly, NMG particles are a magnetic shape memory material with thermoelastic martensitic transformation. According to the results of the phase transition experiments and the variation of the experimental temperature profile, the heat released by hydrate formation can induce the reverse martensitic transformation of NMG particles, while absorbing the surrounding heat, the heat generated by the rapid formation of hydrate induces the reverse martensitic phase transition of NMG, i.e., the transformation from martensitic to austenitic structure occurs, which requires a certain amount of heat absorption and therefore, absorbs the surrounding heat and lowers the system temperature and provides a lower temperature environment for the subsequent rapid hydrate formation. However, micro/nanoparticles have a large specific surface area and high surface energy and are prone to agglomeration and coagulation, leading to precipitation and resistance to dispersion in the base solution, which affects the stability of micro/nanofluids (Liu N et al., 2021). Therefore, the addition of surfactant SDS to the solution can assist in the dispersion of micro/nanoparticles and increase the stability of the nanofluid. Also, SDS can reduce the surface tension at the liquid-phase interface, which can allow methane gas to enter the solution and enhance the solubility of the gas.

In addition, NMG is a material with magnetic function. Under the influence of rotating magnetic field, NMG moves continuously in the solution, driving the liquid to perturb in the reactor and causing random Brownian motion of the fluid, thus improving the energy transfer rate between NMG and base fluid, greatly promoting the mass and heat transfer in the hydrate formation process, and improving the efficiency of gas hydrate formation process. As a result, the gas hydrate generation process becomes more efficient. Figure 10 depicts the mechanism of gas hydrate generation in the NMG system.

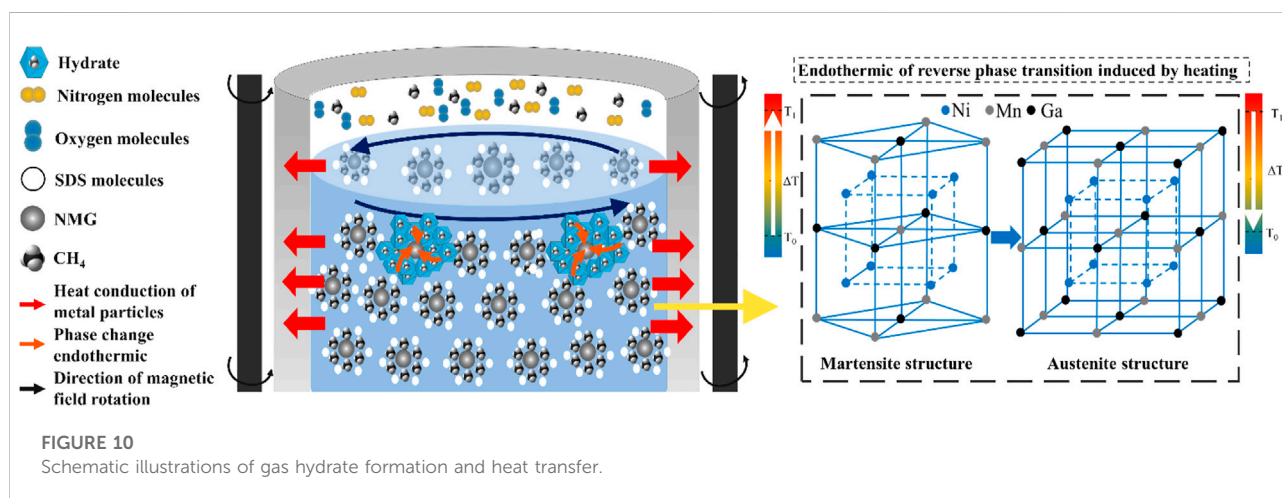


FIGURE 10  
Schematic illustrations of gas hydrate formation and heat transfer.

## 4 Conclusion

NMG was added to a surfactant SDS solution to prepare phase-change micro/nanofluids containing magnetic NMG. This solution system was used to conduct gas hydrate formation studies in an external rotating magnetic field. The NMG-SDS system significantly reduced the induction time of hydrate formation, boosted gas consumption, and improved the gas consumption rate of the gas hydration process, according to the findings. As the initial pressure was 6.2 MPa, the induction time of the NMG-SDS system was reduced by 89.26%, 92.48%, and 95.64%, respectively, when compared to the pure SDS system. The gas consumption increased 3.47%, 7.97%, and 16.43%, respectively; and the average gas consumption rate increased by 5.22%, 7.64%, and 21.88%, respectively. At 6.2 MPa, the maximum gas consumption rates of NMG-SDS in different systems were 0.063, 0.076, and 0.181 mmol min<sup>-1</sup>, respectively, compared with the pure SDS system (0.110, 0.229, and 0.581 mmol of gas/mol of water·min<sup>-1</sup>), which increased 238.18%, 175.55%, and 113.60%, respectively. In addition, the induction time, gas consumption, average gas consumption rate, maximum gas consumption rate, and methane recovery rate increased with increasing initial pressure and methane concentration.

This study's findings serve as a benchmark for the quick development of mixed gas hydrate in NMG systems.

## Data availability statement

The original contributions presented in the study are included in the article/Supplementary Material, further inquiries can be directed to the corresponding author.

## Author contributions

Conceptualization, LL and QW; methodology, FC and BZ; validation, QW; formal analysis, CL; investigation, NL and CL; resources, XX, FC, and QW; data curation, NL; writ-

ing—original draft preparation, NL; writing—review and editing, QW; visualization, QW; supervision, QW; project administration, QW; funding acquisition, QW. All authors have read and agreed to the published version of the manuscript.

## Funding

This research was funded by the National Natural Science Foundation of China under NSFC Contract No. 51804105, U21A20111, 51974112. Additional support was provided by funds from the Fundamental Research Funds for the Central Universities [Grant Number 3072022TS1005] and the University Nursing Program for Young Scholars with Creative Talents in Heilongjiang Province (UNPYSCT-2018096).

## Conflict of interest

The authors declare that the research was conducted in the absence of any commercial or financial relationships that could be construed as a potential conflict of interest.

## Publisher's note

All claims expressed in this article are solely those of the authors and do not necessarily represent those of their affiliated organizations, or those of the publisher, the editors and the reviewers. Any product that may be evaluated in this article, or claim that may be made by its manufacturer, is not guaranteed or endorsed by the publisher.

## Supplementary material

The Supplementary Material for this article can be found online at: <https://www.frontiersin.org/articles/10.3389/fenrg.2022.974647/full#supplementary-material>

## References

- Chaturvedi, E., Laik, S., and Mandal, A. (2021). A comprehensive review of the effect of different kinetic promoters on methane hydrate formation. *Chin. J. Chem. Eng.* 32, 1–16. doi:10.1016/j.cjche.2020.09.027
- Chen, F., Wang, H. B., Meng, X. L., Gao, Z. Y., Cai, W., Zhao, L. C., et al. (2006). Effect of aging on transformation temperatures and microstructure of an Fe-doped Ni-Mn-Ga ferromagnetic shape memory alloy. *Mater. Sci. Eng. A* 438–440, 982–985. doi:10.1016/j.msea.2005.12.045
- Chen, X. (2020). Synergistic Effect of SDS solution and APG solution on gas hydrate formation. *Contemp. Chem. Ind.* 49, 2220. doi:10.13840/j.cnki.cn21-1457/tq.2020.10.027
- Cheng, C., Li, L., Hu, S., Jin, T., Wu, X., Zhang, J., et al. (2021). Study on the enhancement of nucleation and growth of methane hydrate by bubbling. *Refrigeration* 49, 1–7. doi:10.16711/j.1001-7100.2021.02.010
- Cui, W., Sheng, Z., Mao, D., Yang, J., and Wu, S. (2017). Micro-movements of nanoparticles in nanofluids: molecular dynamics simulation. *CIESC J.* 68, 48–53. doi:10.11949/j.issn.0438-1157.20170440
- Fan, J. L., Ai, Y. L., Ou, Y. S., and Zhu, J. W. (2021). Research progress of chemical composition dependence on the thermal and mechanical-magnetic properties of NiMnGa-based alloys. *Rare Metal Mater. Eng.* 50, 4185–4192.
- Gaikwad, N., Sangwai, J., Linga, P., and Kumar, R. (2021). Separation of coal mine methane gas mixture via sII and sH hydrate formation. *Fuel* 305, 121467–467. doi:10.1016/j.fuel.2021.121467
- Gao, Q., Li, A., Chen, X., Lu, N., Zhang, Y., and Chen, L. (2021). A microporous metal-organic framework with triangular channels for C<sub>2</sub>H<sub>6</sub>/C<sub>2</sub>H<sub>4</sub> adsorption separation. *Sep. Purif. Technol.* 276, 119424. doi:10.1016/j.seppur.2021.119424

- George, A., Shen, B., Kang, D., Yang, J., and Luo, J. (2020). Emission control strategies of hazardous trace elements from coal-fired power plants in China. *J. Environ. Sci.* 93, 66–90. doi:10.1016/j.jes.2020.02.025
- Huang, X., Cong, H., Jin, Y., Yin, S., Xia, B., and Ma, G. (2021). Effect of silica-SDS complex system on methane hydrate formation process. *Mod. Chem. Ind.* 41, 6. doi:10.16606/j.cnki.issn0253-4320.2021.08.020
- Jiang, C., Liu, J., Wang, J., Xu, L., and Xu, H. (2004). Solid-liquid interface morphology and crystal growth of NiMnGa magnetic shape memory alloys. *Acta Mater.* 53 (4), 1111–1120. doi:10.1016/j.actamat.2004.11.008
- Jiang, X., Chuah, C., Goh, K., and Wang, R. (2021). A facile direct spray-coating of Pebax® 1657: Towards large-scale thin-film composite membranes for efficient CO<sub>2</sub>/N<sub>2</sub> separation. *J. Memb. Sci.* 638, 119708. doi:10.1016/j.memsci.2021.119708
- Liu, N., Hong, C., and Liu, X. (2017). Effects of nanoparticles on CO<sub>2</sub> hydrate thermal conductivity. *Huagong Xuebao/CIESC J.* 68, 3404–3408. doi:10.11949/j.issn.0438-1157.201616665
- Liu, N., Zhu, H. Q., Zhou, J. L., Yang, L., and Liu, D. P. (2021). Molecular dynamics simulations on formation of CO<sub>2</sub> hydrate in the presence of metal particles. *J. Mol. Liq.* 331, 115793. doi:10.1016/j.molliq.2021.115793
- Liu, Z., Li, Y., Wang, W., Song, G., Lu, Z., Ning, Y., et al. (2021). Experimental investigation on the micro-morphologies and growing process of methane hydrate formation in SDS solution. *Fuel* 293, 120320. doi:10.1016/j.fuel.2021.120320
- Liu, Z., Yang, L., Liu, D., and Xie, Y. (2020). Natural gas hydrates formation in the metal nanoparticles and fibers suspension. *Shanghai Ligong Daxue Xuebao/Journal Univ. Shanghai Sci. Technol.* 42, 232–239. doi:10.13255/j.cnki.jusst.20190311005
- Lyubina, J. (2017). Magnetocaloric materials for energy efficient cooling. *J. Phys. D. Appl. Phys.* 50, 053002. doi:10.1088/1361-6463/50/5/053002
- Kang, G. Z., Kan, Q. H., Yu, C., and Song, D. (2018). Study on cyclic deformation and fatigue of thermal and magnetic shape memory alloys. *J. Adv. Mechanics.* 48 (1), 1802. doi:10.6052/1000-0992-17-008
- Manfred, W., Corneliu, C., and Jian, L. (2000). Phase transformations in ferromagnetic NiMnGa shape memory films. *Mat. Trans. JIM* 41 (8), 933–937. doi:10.2320/matertrans1989.41.933
- Pahlavanzadeh, H., Rezaei, S., Khanlarkhani, M., Manteghian, M., and Mohammadi, A. H. (2016). Kinetic study of methane hydrate formation in the presence of copper nanoparticles and CTAB. *J. Nat. Gas. Sci. Eng.* 34, 803–810. doi:10.1016/j.jngse.2016.07.001
- Ren, S., Liu, J., Liu, Y., Fan, Z., Liu, Y., Zuo, J., et al. (2020). Experimental study on formation and dissociation of methane hydrate in porous media. *Shiyou Xuebao/Acta Pet. Sin.* 30, 583. doi:10.3321/j.issn:0253-2697.2009.04.019
- Smith, J. M., Ness, H. C., and Van Abbott, M. M. (2001). *Introduction to chemical engineering thermodynamics*. New York: McGraw-Hill.
- Song, Y. M., Liang, R. Q., Wang, F., Zhang, D. H., Yang, L., and Zhang, D. B. (2021). Enhanced methane hydrate formation in the highly dispersed carbon nanotubes-based nanofluid. *Fuel* 285, 119234. doi:10.1016/j.fuel.2020.119234
- Su, F., Ma, X., and Chen, J. (2008). Han ZX, Experimental study on enhancement of bubble absorption with binary nanofluid. *J. Refrig.* 29, 8–12. doi:10.3969/j.issn.0253-4339.2008.01.002
- Sun, J. Y., Xie, Y. M., Xu, Z. T., Yang, Y. X., and Chen, J. W. (2019). Research progress in nanofluids-enhanced formation of CO<sub>2</sub> hydrate. *Mod. Chem. Ind.* 39, 26–30. doi:10.16606/j.cnki.issn0253-4320.2019.12.006
- Sun, S., and Fan, S. (2005). The formation of natural gas hydrates with ultrasonic. *Chem. East.* 68 (11), 867–870. doi:10.14159/j.cnki.0441-3776.2005.11.011
- Tian, B., Chen, F., Tong, Y. X., Li, L., and Zheng, Y. F. (2009). Research progress in NiMnGa ferromagnetic shape memory alloy Particles/Polymer smart composite. *Mater. Rep.* 23 (05), 9–12+21. doi:10.3321/j.issn:1005-023X.2009.05.003
- Tian, J., Shen, Y., Zhang, D., and Tang, Z. (2021). CO<sub>2</sub> capture by vacuum pressure swing adsorption from dry flue gas with a structured composite adsorption medium. *J. Environ. Chem. Eng.* 9, 106037. doi:10.1016/j.jece.2021.106037
- Veluswamy, H., Kumar, A., Seo, Y., Lee, J., and Linga, P. (2018). A review of solidified natural gas (SNG) technology for gas storage via clathrate hydrates. *Appl. Energy* 216, 262–285. doi:10.1016/j.apenergy.2018.02.059
- Wu, Y. J., Tang, T. Q., Shi, L., and He, Y. R. (2021). Rapid hydrate-based methane storage promoted by bilayer surfactant-coated Fe<sub>3</sub>O<sub>4</sub> nanoparticles under a magnetic field. *Fuel* 303, 121248. doi:10.1016/j.fuel.2021.121248
- Xia, G. D., Liu, R., and Du, M. (2016). Analysis of the thermal conductivity of nanofluids. *J. Beijing Univ. Technol.* 42, 1252–1258. doi:10.11936/bjtxb2015100029
- Yang, Z., Lu, B., Guo, D., Ji, Z., Ji, C., and Zhang, G. (2020). Research status and progress of CO<sub>2</sub> capture and separation methods. *Shandong Chem. Ind.* 49 (18), 2. doi:10.19319/j.cnki.issn.1008-021x.2020.18.023
- Yi, J., Zhong, D., Yan, J., and Lu, Y. (2019). Impacts of the surfactant sulfonated lignin on hydrate based CO<sub>2</sub> capture from a CO<sub>2</sub>/CH<sub>4</sub> gas mixture. *Energy* 171, 61–68. doi:10.1016/j.energy.2019.01.007
- Yin, S. W., Jin, Y., Xia, B., and Ma, G. Y. (2020). Study on the characteristics of the effect of the synergistic system of calcium carbonate and SDS on the formation of methane hydrate. *J. Petrochem. Univ.* 33, 64–70. doi:10.3969/j.issn.1006-396X.2020.06.011
- Yoslim, J., Linga, P., and Englezos, P. (2010). Enhanced growth of methane-propane clathrate hydrate crystals with sodium dodecyl sulfate, sodium tetradecyl sulfate, and sodium hexadecyl sulfate surfactants. *J. Cryst. Growth* 313, 68–80. doi:10.1016/j.jcrysgro.2010.10.009
- Yu, S. Y., Cao, Z. X., Ma, L., Liu, G. D., Chen, J. L., Wu, G. H., et al. (2007). Realization of magnetic field-induced reversible martensitic transformation in NiCoMnGa alloys. *Appl. Phys. Lett.* 91, 102507–102513. doi:10.1063/1.2783188
- Yuan, L. (2021). Research progress of mining response and disaster prevention and control in deep coal mines. *J. China Coal Soc.* 46, 716–724. doi:10.13225/j.cnki.jccs.YT21.0158
- Zhang, G., Liu, B., Xu, L., Zhang, R., He, Y., and Wang, F. (2021a). How porous surfaces influence the nucleation and growth of methane hydrates. *Fuel* 291, 120142. doi:10.1016/j.fuel.2021.120142
- Zhang, G., Zhang, R., and Wang, F. (2021b). Fast formation kinetics of methane hydrates loaded by silver nanoparticle coated activated carbon (Ag-NP@AC). *Chem. Eng. J.* 417, 129206. doi:10.1016/j.cej.2021.129206
- Zhang, Q., Wu, Q., Zhang, H., Zhang, B., and Xia, T. (2018). Effect of montmorillonite on hydrate-based methane separation from mine gas. *J. Cent. South Univ.* 25, 38–50. doi:10.1007/s11771-018-3715-x
- Zhang, Z., Liu, Z., Pan, Z., Baena-Moreno, F., and Soltanian, M. (2020). Effect of porous media and its distribution on methane hydrate formation in the presence of surfactant. *Appl. Energy* 261, 114373. doi:10.1016/j.apenergy.2019.114373
- Zhong, D., Yang, C., Liu, D., and Wu, Z. (2010). Experimental study on formation of carbon dioxide hydrate in a water spraying reactor. *Chin. J. Process Eng.* 10.
- Zhou, J. (2016). Dissipative particle dynamics and navier boundary condition simulations in micro-and nanofluids. *Acta Polym. Sin.* 8, 1021–1029. doi:10.11777/j.issn1000-3304.2016.16070
- Zhou, S. D., Yu, Y. S., Zhang, J., Wang, S. L., Zhao, S. H., and Li, H. (2014). Research development of nanofluid-strengthened hydrate formation. *Mod. Chem. Ind.* 34, 51–56.